Numerical Simulation of Marangoni Convection in Consideration of Free Surface Displacement

By
Takanori Hashimoto[1], Yukifumi Kousaka[1], Ichiro Ueno[1], Hiroshi Kawamura[1] and Shinichi Yoda[2]

Abstract: Thermocapillary-driven convection in a half-zone liquid bridge has been extensively examined. A large number of researches have been conducted concerning the transition of the flow field. Physical mechanism of the transition, however, has not been fully understood. In the present study, three-dimensional numerical simulations taking with and without dynamic free surface deformation (DSD) into account are carried out to evaluate the effect of the surface deformation upon the flow field. The surface shape is solved by considering the stress balance on the free surface, and the calculation coordinate is reconstructed at every time step with employing a boundary fitted coordinate. The test fluids are acetone (Pr=4.38) and 2cSt silicone oil (Pr=28.11). The free surface deformation is determined primarily by the pressure variation. For acetone, the effect of the DSD upon critical point and flow field was quite small in the range of present numerical simulation in previous report. In this report, the effect of DSD for 2cSt silicone oil is obtained.

1. INTRODUCTION

One of the purposes of the space environment utilization is the processing of a new material, because the buoyancy effect can be reduced in the space environment. Floating-zone method is one of the well-known material processing methods under the micro-gravity. In this method, however, the convection, still occurs induced by the surface tension difference on the free surface owing to the temperature gradient. This convection is called thermocapillary or Marangoni convection and has been widely investigated with a half-zone (HZ) model corresponding to half part of floating-zone model. In the HZ model, a liquid bridge is sustained between the coaxial cylindrical rods. Each rod is maintained at different temperature, thus the liquid bridge is exposed by a temperature difference ΔT between the both rods. When ΔT exceeds a critical value ΔT_c, the induced flow in the HZ bridge of medium and high Prandtl number fluid exhibit a transition from a two-dimensional steady flow to a three-dimensional oscillatory one. The oscillatory flow has two patterns called as 'Standing wave' and 'Traveling wave'. These flows appear depending upon the temperature difference. The structure in the liquid bridge is characterized further by the azimuthal wave number m. The flow field is divided azimuthally into 2×m sectors; the alternate sector, m in total, consists of the same thermal-fluid structure.

The experiments for the thermocapillary convection have been widely conducted. Preisser et al. (1983) [1] investigated the oscillatory flow to study the effect of several parameters such as the aspect ratio and Marangoni number. Velten et al. (1991) [2] observed the periodic instability of thermocapillary convection in the cylindrical liquid bridge.

[1]Tokyo University of Science, 2641 Yamazaki, Noda-shi, Chiba 278-8510, Japan
[2]JAXA, 2-1-1 Sengen, Tsukuba City, 305-8505,Japan

As for the numerical simulation, Kuhlmann (1993)[3], Wanschura et al. (1995)[4] calculated the critical Reynolds number for the various non-dimensional numbers (Bi, Gr, Pr, A) using the linear stability analysis. Savino and Monti (1996) [5] simulated the oscillatory flow numerically and compared it with their experiments. Shevtsova et al. (1998) [6] studied the transition from two dimensional thermoconvective steady flow to a time-dependent flow considered for an axisymmetric liquid bridge of a high Prandtl number fluid (Pr = 105) with a static curved free surface.

It should be noted that most of the existing numerical simulations were conducted without considering the dynamic free surface movement. After the onset of oscillation, however, the pressure field fluctuates violently because of the unsteady flow. Therefore the free surface is expected to dynamically deform due to these fluctuation. In fact, the free surface vibration in the liquid bridge has been observed in some terrestrial experiments. Kamotani et al. (2000) [7] reported an experiment of the thermocapillary convection performed aboard the Spacelab in an open cylindrical container, and investigated the free surface movement. In addition, they analyzed the influence of surface deformation upon the critical condition in the half-zone configuration. Correlation between the criticality and the dynamic surface deformation, however, is not understood yet. An influence of surface vibration upon the flow field instability must be evaluated to understand the mechanism of the oscillatory flow. To the authors' knowledge, no numerical work has been done on the thermocapillary convection in a liquid bridge with including the dynamic deformation of the surface.

Recently, Kuhlmann et al. [8] have made a combined analytical and numerical study on the thermocapillary convection in a liquid bridge with including the DSD using the linear stability analysis. They analyzed the mutual relation between the flow field and the dynamic surface deformation of the most dangerous mode. The present study aims at understanding time-dependent thermal-fluid phenomena with dynamic free surface deformation in the half-zone liquid bridge by a direct nonlinear numerical simulation.

2. NOMENCLATURES

Γ	aspect ratio
D	diameter
g	gravity
h	heat transfer coefficient
H	height of the liquid bridge
I	unit matrix
J	Jacobian
m	azimuthal wave number
n	surface-normal vector
N	normalizing dominator
P	pressure
$r,\ \theta\ , z$	coordinates
$\xi\ ,\ \zeta\ ,\ \eta$	coordinates in the computational domain
$R,\ R_k$	position of the free surface
R_0	radius of the disk
$R_{1,\ 2}$	main radii of curvature
S	stress tensor
t	time
T	temperature
T_0	reference temperature
U_0	maximum velocity
$V_{r,\ \theta\ ,z},\ V_{x,y}$	velocities
v_i	compensated temporally velocity
v_i	temporally velocity
V	volume of the liquid bridge
$V_{\xi\ ,\ \zeta\ ,\ \eta}$	contravariant velocities
$V_{\xi\ ,\ \zeta\ ,\ \eta}$	temporally contravariant velocities
α	contact angle
β	thermal expansion coefficient
$\Delta\ T$	temperature difference between the disks
$\delta\ s$	amount of free surface deformation
τ	time in the computational domain
$\sigma\ ,\ \sigma\ (\ T)$	surface tension
$\sigma\ 0(\ T0)$	reference surface tension
$\sigma\ T$	thermal coefficient of surface tension
κ	thermal diffusivity
λ	thermal conductivity
μ	dynamic viscosity
ν	kinematic viscosity
ρ	density
Bi	Biot number
Bo	Bond number
Ca	Capillary number
Gr	Grashof number
Ma	Marangoni number
Pr	Prandtl number
Re	Reynolds number

3. NUMERICAL METHOD

The purpose of this study is to analyze the influence of the free surface deformation upon the thermocapillary flow. Therefore, a numerical method to capture the temporally varying surface motion is employed. The deformed surface is expressed using the boundary fitted coordinate (BFC).

To consider the thermocapillary convection in a liquid bridge, a configuration of the analysis is defined as shown in Fig. 1. The liquid bridge with volume V_0 is sustained by two rigid parallel disks of equal radii $r = R_0$ located at $z = 0$ and H. The temperature difference between these disks is defined by ΔT.

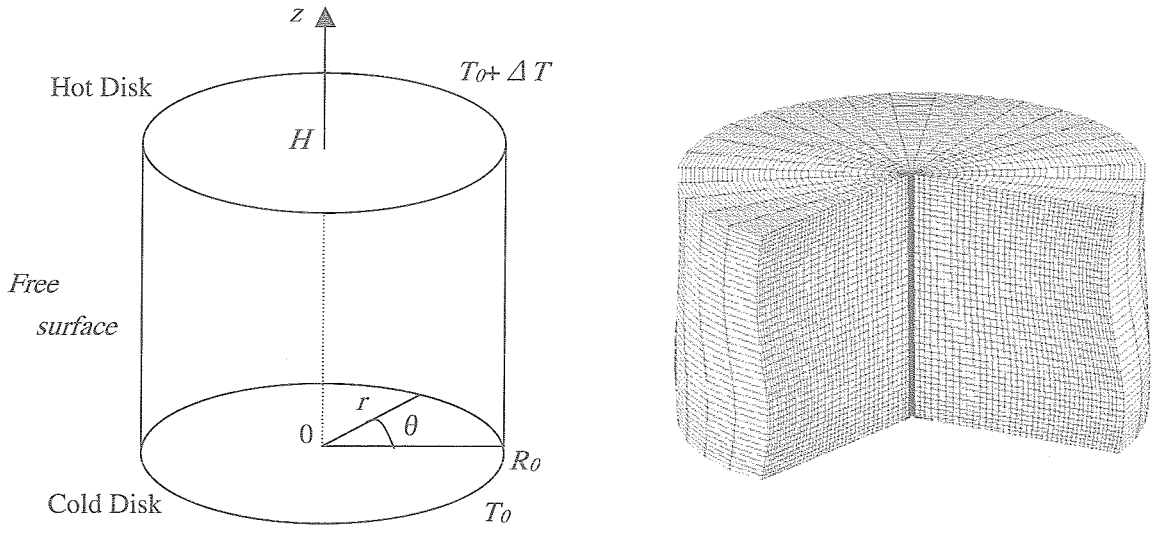

Figure 1: Numerical configuration

3.1 Governing equations

The liquid is assumed to be an incompressible Newtonian fluid of kinematic viscosity ν and density ρ. In a cylindrical coordinates system, the continuity, the Navier-Stokes and the energy equations are given by

$$\nabla \cdot \mathbf{u} = 0 \tag{1}$$

$$\frac{\partial \mathbf{u}}{\partial t} + (\mathbf{u} \cdot \nabla)\mathbf{u} = -\nabla P + \frac{Pr}{Ma}\nabla^2 \mathbf{u} \tag{2}$$

$$\frac{\partial T}{\partial t} + (\mathbf{u} \cdot \nabla)T = \frac{1}{Ma}\nabla^2 T \tag{3}$$

Variables are non-dimensionalized using scales as Table 1.

Table 1: Scales used for non-dimensionalization

Variable	r, z	t	$v = (v_r, v_\theta, v_z)$	p	T
Scale	H	$H\mu / \sigma_T \Delta T$	$\sigma_T \Delta T / \rho$	$\rho (\sigma_T \Delta T / \mu)^2$	ΔT

The non-dimensional numbers are defined by

$$Re = \frac{U_0 H}{\nu}$$

$$Pr = \frac{\nu}{\kappa}$$

$$Ma = \frac{1}{\mu\kappa}\left|\frac{\partial\sigma}{\partial T}\right|\Delta T \cdot H$$

3.2 Boundary fitted coordinate

The shape of the liquid bridge is deformed dynamically in this calculation. Therefore, the adequate coordinate system must be employed to calculate the flow field with the finite difference method. The boundary fitted coordinate method is applied to the governing equations in all directions. In the previous study, the computational domain was assumed to be cubic. The substantial error arises in the conversion from the cylinder in the physical domain to the cubic in the computational one. Thus, the present computational domain is modified to cylindrical coordinate. Equations (1)-(3) can be transformed from the physical domain to the computational domain by Jacobian matrix.

$$\begin{bmatrix} \frac{\partial}{\partial t} \\ \frac{\partial}{\partial r} \\ \frac{\partial}{\partial \theta} \\ \frac{\partial}{\partial z} \end{bmatrix} = \begin{bmatrix} 1 & \xi_t & \zeta_t & \eta_t \\ 0 & \xi_r & \zeta_r & \eta_r \\ 0 & \xi_\theta & \zeta_\theta & \eta_\theta \\ 0 & \xi_z & \zeta_z & \eta_z \end{bmatrix} \begin{bmatrix} \frac{\partial}{\partial \tau} \\ \frac{\partial}{\partial \xi} \\ \frac{\partial}{\partial \zeta} \\ \frac{\partial}{\partial \eta} \end{bmatrix} \tag{4}$$

$$\begin{bmatrix} \frac{\partial}{\partial \tau} \\ \frac{\partial}{\partial \xi} \\ \frac{\partial}{\partial \zeta} \\ \frac{\partial}{\partial \eta} \end{bmatrix} = \begin{bmatrix} 1 & r_\tau & \theta_\tau & z_\tau \\ 0 & r_\xi & \theta_\xi & z_\xi \\ 0 & r_\zeta & \theta_\zeta & z_\zeta \\ 0 & r_\eta & \theta_\eta & z_\eta \end{bmatrix} \begin{bmatrix} \frac{\partial}{\partial t} \\ \frac{\partial}{\partial r} \\ \frac{\partial}{\partial \theta} \\ \frac{\partial}{\partial z} \end{bmatrix} \tag{5}$$

Equation (5) is inversely transformed as follows,

$$\begin{bmatrix} \frac{\partial}{\partial t} \\ \frac{\partial}{\partial r} \\ \frac{1}{r}\frac{\partial}{\partial \theta} \\ \frac{\partial}{\partial z} \end{bmatrix} = \frac{1}{J}\begin{bmatrix} A_{11} & A_{12} & A_{13} & A_{14} \\ A_{21} & A_{22} & A_{23} & A_{24} \\ A_{31} & A_{32} & A_{33} & A_{34} \\ A_{41} & A_{42} & A_{43} & A_{44} \end{bmatrix}\begin{bmatrix} \frac{\partial}{\partial \tau} \\ \frac{\partial}{\partial \xi} \\ \frac{1}{\xi}\frac{\partial}{\partial \zeta} \\ \frac{\partial}{\partial \eta} \end{bmatrix} \tag{6}$$

where,

$$A_{11} = \frac{r}{\xi}\left(r_\xi\theta_\zeta z_\eta + r_\zeta\theta_\eta z_\xi + r_\eta\theta_\xi z_\zeta - r_\eta\theta_\zeta z_\xi - r_\zeta\theta_\xi z_\eta - r_\xi\theta_\eta z_\zeta\right),$$

$$A_{12} = -\frac{r}{\xi}\left(r_\tau\theta_\zeta z_\eta + r_\zeta\theta_\eta z_\tau + r_\eta\theta_\tau z_\zeta - r_\eta\theta_\zeta z_\tau - r_\zeta\theta_\tau z_\eta - r_\tau\theta_\eta z_\zeta\right),$$

$$A_{13} = r\left(r_\tau\theta_\xi z_\eta + r_\xi\theta_\eta z_\tau + r_\eta\theta_\tau z_\xi - r_\eta\theta_\xi z_\tau - r_\xi\theta_\tau z_\eta - r_\tau\theta_\eta z_\xi\right),$$

$$A_{14} = -\frac{r}{\xi}\left(r_\tau\theta_\xi z_\zeta + r_\xi\theta_\zeta z_\tau + r_\zeta\theta_\tau z_\xi - r_\zeta\theta_\xi z_\tau - r_\xi\theta_\tau z_\zeta - r_\tau\theta_\zeta z_\xi\right),$$

$$A_{21} = 0 \quad A_{22} = \frac{r}{\xi}\left(\theta_\zeta z_\eta - \theta_\eta z_\zeta\right), \quad A_{23} = -r\left(\theta_\xi z_\eta - \theta_\eta z_\xi\right), \quad A_{24} = \frac{r}{\xi}\left(\theta_\xi z_\zeta - \theta_\zeta z_\xi\right),$$

$$A_{31} = 0 \quad A_{32} = -\frac{1}{\xi}\left(r_\zeta z_\eta - r_\eta z_\zeta\right), \quad A_{33} = \left(r_\xi z_\eta - r_\eta z_\xi\right), \quad A_{34} = -\frac{1}{\xi}\left(r_\xi z_\zeta - r_\zeta z_\xi\right),$$

$$A_{41} = 0 \quad A_{42} = \frac{r}{\xi}\left(r_\zeta\theta_\eta - r_\eta\theta_\zeta\right), \quad A_{43} = -r\left(r_\xi\theta_\eta - r_\eta\theta_\xi\right), \quad A_{44} = \frac{r}{\xi}\left(r_\xi\theta_\zeta - r_\zeta\theta_\xi\right).$$

Each component can be related from Eqs. (4) and (6) as:

$$J = \frac{r}{\xi}\left(r_\xi\theta_\zeta z_\eta + r_\zeta\theta_\eta z_\xi + r_\eta\theta_\xi z_\zeta - r_\eta\theta_\zeta z_\xi - r_\zeta\theta_\xi z_\eta - r_\xi\theta_\eta z_\zeta\right),$$

$$\xi_t = -\frac{1}{J}\frac{r}{\xi}\left(r_\tau\theta_\zeta z_\eta + r_\zeta\theta_\eta z_\tau + r_\eta\theta_\tau z_\zeta - r_\eta\theta_\zeta z_\tau - r_\zeta\theta_\tau z_\eta - r_\tau\theta_\eta z_\zeta\right),$$

$$\zeta_t = \frac{1}{J}r\left(r_\tau\theta_\xi z_\eta + r_\xi\theta_\eta z_\tau + r_\eta\theta_\tau z_\xi - r_\eta\theta_\xi z_\tau - r_\xi\theta_\tau z_\eta - r_\tau\theta_\eta z_\xi\right),$$

$$\eta_t = -\frac{1}{J}\frac{r}{\xi}\left(r_\tau\theta_\xi z_\zeta + r_\xi\theta_\zeta z_\tau + r_\zeta\theta_\tau z_\xi - r_\zeta\theta_\xi z_\tau - r_\xi\theta_\tau z_\zeta - r_\tau\theta_\zeta z_\xi\right)$$

$$\xi_r = \frac{1}{J}\frac{r}{\xi}\left(\theta_\zeta z_\eta - \theta_\eta z_\zeta\right), \quad \zeta_r = -\frac{1}{J}r\left(\theta_\xi z_\eta - \theta_\eta z_\xi\right), \quad \eta_r = \frac{1}{J}\frac{r}{\xi}\left(\theta_\xi z_\zeta - \theta_\zeta z_\xi\right),$$

$$\xi_\theta = -\frac{1}{J}\frac{1}{\xi}\left(r_\zeta z_\eta - r_\eta z_\zeta\right), \quad \zeta_\theta = \frac{1}{J}\left(r_\xi z_\eta - r_\eta z_\xi\right), \quad \eta_\theta = -\frac{1}{J}\frac{1}{\xi}\left(r_\xi z_\zeta - r_\zeta z_\xi\right),$$

$$\xi_z = \frac{1}{J}\frac{r}{\xi}\left(r_\zeta\theta_\eta - r_\eta\theta_\zeta\right), \quad \zeta_z = -\frac{1}{J}r\left(r_\xi\theta_\eta - r_\eta\theta_\xi\right), \quad \eta_z = \frac{1}{J}\frac{r}{\xi}\left(r_\xi\theta_\zeta - r_\zeta\theta_\xi\right).$$

The continuity, the Navier- Stokes and the energy equations (Eqs. (1)-(3)) are transformed to the ones in the generalized coordinates.

[Continuity equation]

$$\frac{1}{\xi}\frac{\partial}{\partial\xi}\left(J\xi V_\xi\right)+\frac{1}{\xi}\frac{\partial}{\partial\zeta}\left(JV_\zeta\right)+\frac{\partial}{\partial\eta}\left(JV_\eta\right)=0 \tag{7}$$

where

$$V_\xi=\xi_r v_r+\frac{1}{r}\xi_\theta v_\theta+\xi_z v_z,\quad V_\zeta=\xi\zeta_r v_r+\frac{1}{r}\xi\zeta_\theta v_\theta+\xi\zeta_z v_z,\quad V_\eta=\eta_r v_r+\frac{1}{r}\eta_\theta v_\theta+\eta_z v_z.$$

These velocities are called as contravariant velocities.

[Navier-Stokes equation]

$$\frac{\partial v_i}{\partial t}+\xi_t\frac{\partial v_i}{\partial\xi}+\zeta_t\frac{\partial v_i}{\partial\zeta}+\eta_t\frac{\partial v_i}{\partial\eta}$$
$$+\frac{1}{J}\left[\frac{1}{\xi}\frac{\partial}{\partial\xi}\left(J\xi V_\xi v_i\right)+\frac{1}{\xi}\frac{\partial}{\partial\zeta}\left(JV_\zeta v_i\right)+\frac{\partial}{\partial\eta}\left(JV_\eta v_i\right)+e_r\left(-\frac{Jv_\theta^2}{r}\right)+e_\theta\left(\frac{Jv_r v_\theta}{r}\right)\right]$$

$$=-\left(\xi_i\frac{\partial P}{\partial\xi}+\zeta_i\frac{\partial P}{\partial\zeta}+\eta_i\frac{\partial P}{\partial\eta}\right)e_i$$
$$+\frac{Pr}{Ma}\frac{1}{J}\left[\begin{array}{l}
\frac{1}{\xi}\frac{\partial}{\partial\xi}\left(J\xi\xi_r\xi_r\frac{\partial v_i}{\partial\xi}\right)+\frac{1}{\xi}\frac{\partial}{\partial\xi}\left(J\xi\xi_r\zeta_r\frac{\partial v_i}{\partial\zeta}\right)+\frac{1}{\xi}\frac{\partial}{\partial\xi}\left(J\xi\xi_r\eta_r\frac{\partial v_i}{\partial\eta}\right)\\
+\ \frac{1}{\xi}\frac{\partial}{\partial\zeta}\left(J\xi\zeta_r\xi_r\frac{\partial v_i}{\partial\xi}\right)+\frac{\partial}{\partial\zeta}\left(J\xi\zeta_r\zeta_r\frac{\partial v_i}{\partial\zeta}\right)+\frac{\partial}{\partial\zeta}\left(J\xi\zeta_r\eta_r\frac{\partial v_i}{\partial\eta}\right)\\
+\ \frac{\partial}{\partial\eta}\left(J\eta_r\xi_r\frac{\partial v_i}{\partial\xi}\right)+\frac{\partial}{\partial\eta}\left(J\eta_r\zeta_r\frac{\partial v_i}{\partial\zeta}\right)+\frac{\partial}{\partial\eta}\left(J\eta_r\eta_r\frac{\partial v_i}{\partial\eta}\right)\\
+\ \frac{\partial}{\partial\xi}\left(J\frac{1}{r^2}\xi_\theta\xi_\theta\frac{\partial v_i}{\partial\xi}\right)+\frac{\partial}{\partial\xi}\left(J\frac{1}{r^2}\xi_\theta\zeta_\theta\frac{\partial v_i}{\partial\zeta}\right)+\frac{\partial}{\partial\xi}\left(J\frac{1}{r^2}\xi_\theta\eta_\theta\frac{\partial v_i}{\partial\eta}\right)\\
+\ \frac{1}{\xi}\frac{\partial}{\partial\zeta}\left(J\frac{\xi}{r^2}\zeta_\theta\xi_\theta\frac{\partial v_i}{\partial\xi}\right)+\frac{1}{\xi}\frac{\partial}{\partial\zeta}\left(J\frac{\xi}{r^2}\zeta_\theta\zeta_\theta\frac{\partial v_i}{\partial\zeta}\right)+\frac{1}{\xi}\frac{\partial}{\partial\zeta}\left(J\frac{\xi}{r^2}\zeta_\theta\eta_\theta\frac{\partial v_i}{\partial\eta}\right)\\
+\ \frac{\partial}{\partial\eta}\left(J\frac{1}{r^2}\eta_\theta\xi_\theta\frac{\partial v_i}{\partial\xi}\right)+\frac{\partial}{\partial\eta}\left(J\frac{1}{r^2}\eta_\theta\zeta_\theta\frac{\partial v_i}{\partial\zeta}\right)+\frac{\partial}{\partial\eta}\left(J\frac{1}{r^2}\eta_\theta\eta_\theta\frac{\partial v_i}{\partial\eta}\right)\\
+\ \frac{1}{\xi}\frac{\partial}{\partial\xi}\left(J\xi\xi_z\xi_z\frac{\partial v_i}{\partial\xi}\right)+\frac{\partial}{\partial\xi}\left(J\xi\xi_z\zeta_z\frac{\partial v_i}{\partial\zeta}\right)+\frac{\partial}{\partial\xi}\left(J\xi\xi_z\eta_z\frac{\partial v_i}{\partial\eta}\right)\\
+\ \frac{1}{\xi}\frac{\partial}{\partial\zeta}\left(J\xi\zeta_z\xi_z\frac{\partial v_i}{\partial\xi}\right)+\frac{\partial}{\partial\zeta}\left(J\xi\zeta_z\zeta_z\frac{\partial v_i}{\partial\zeta}\right)+\frac{\partial}{\partial\zeta}\left(J\xi\zeta_z\eta_z\frac{\partial v_i}{\partial\eta}\right)
\end{array}\right.$$

$$
\begin{aligned}
&+ \frac{\partial}{\partial\eta}\left(J\eta_z\xi_z\frac{\partial v_i}{\partial\xi}\right)+\frac{\partial}{\partial\eta}\left(J\eta_z\zeta_z\frac{\partial v_i}{\partial\zeta}\right)+\frac{\partial}{\partial\eta}\left(J\eta_z\eta_z\frac{\partial v_i}{\partial\eta}\right)\\
&+ e_r\left(-J\frac{v_r}{r^2}-J\frac{2}{r^2}\left(\frac{1}{r}\xi_\theta\frac{\partial v_\theta}{\partial\xi}+\frac{1}{r}\zeta_\theta\frac{\partial v_\theta}{\partial\zeta}+\frac{1}{r}\eta_\theta\frac{\partial v_\theta}{\partial\eta}\right)\right)\\
&+ e_\theta\left(-J\frac{v_\theta}{r^2}-J\frac{2}{r^2}\left(\frac{1}{r}\xi_\theta\frac{\partial v_r}{\partial\xi}+\frac{1}{r}\zeta_\theta\frac{\partial v_r}{\partial\zeta}+\frac{1}{r}\eta_\theta\frac{\partial v_r}{\partial\eta}\right)\right)\ \Bigg]\\
&+ e_z\left(\frac{Gr}{Re^2}T\right)
\end{aligned}
\tag{8}
$$

where, $v_i = (v_r, v_\theta, v_z)$.

[Energy equation]

$$
\begin{aligned}
&\frac{\partial T}{\partial t}+\xi_t\frac{\partial T}{\partial\xi}+\zeta_t\frac{\partial vT}{\partial\zeta}+\eta_t\frac{\partial T}{\partial\eta}\\
&+\frac{1}{J}\left[\frac{1}{\xi}\frac{\partial}{\partial\xi}\left(J\xi V_\xi T\right)+\frac{1}{\xi}\frac{\partial}{\partial\zeta}\left(JV_\zeta T\right)+\frac{\partial}{\partial\eta}\left(JV_\eta T\right)\right]
\end{aligned}
$$

$$
\begin{aligned}
= \frac{1}{Ma}\frac{1}{J}\Bigg[\ &\frac{1}{\xi}\frac{\partial}{\partial\xi}\left(J\xi\xi_r\xi_r\frac{\partial T}{\partial\xi}\right)+\frac{1}{\xi}\frac{\partial}{\partial\xi}\left(J\xi\xi_r\zeta_r\frac{\partial T}{\partial\zeta}\right)+\frac{1}{\xi}\frac{\partial}{\partial\xi}\left(J\xi\xi_r\eta_r\frac{\partial T}{\partial\eta}\right)\\
&+\frac{1}{\xi}\frac{\partial}{\partial\zeta}\left(J\xi\zeta_r\xi_r\frac{\partial T}{\partial\xi}\right)+\frac{\partial}{\partial\zeta}\left(J\xi\zeta_r\zeta_r\frac{\partial T}{\partial\zeta}\right)+\frac{\partial}{\partial\zeta}\left(J\xi\zeta_r\eta_r\frac{\partial T}{\partial\eta}\right)\\
&+\frac{\partial}{\partial\eta}\left(J\eta_r\xi_r\frac{\partial T}{\partial\xi}\right)+\frac{\partial}{\partial\eta}\left(J\eta_r\zeta_r\frac{\partial T}{\partial\zeta}\right)+\frac{\partial}{\partial\eta}\left(J\eta_r\eta_r\frac{\partial T}{\partial\eta}\right)\\
&+\frac{\partial}{\partial\xi}\left(J\frac{1}{r^2}\xi_\theta\xi_\theta\frac{\partial T}{\partial\xi}\right)+\frac{\partial}{\partial\xi}\left(J\frac{1}{r^2}\xi_\theta\zeta_\theta\frac{\partial T}{\partial\zeta}\right)+\frac{\partial}{\partial\xi}\left(J\frac{1}{r^2}\xi_\theta\eta_\theta\frac{\partial T}{\partial\eta}\right)\\
&+\frac{1}{\xi}\frac{\partial}{\partial\zeta}\left(J\frac{\xi}{r^2}\zeta_\theta\xi_\theta\frac{\partial T}{\partial\xi}\right)+\frac{1}{\xi}\frac{\partial}{\partial\zeta}\left(J\frac{\xi}{r^2}\zeta_\theta\zeta_\theta\frac{\partial T}{\partial\zeta}\right)+\frac{1}{\xi}\frac{\partial}{\partial\zeta}\left(J\frac{\xi}{r^2}\zeta_\theta\eta_\theta\frac{\partial T}{\partial\eta}\right)\\
&+\frac{\partial}{\partial\eta}\left(J\frac{1}{r^2}\eta_\theta\xi_\theta\frac{\partial T}{\partial\xi}\right)+\frac{\partial}{\partial\eta}\left(J\frac{1}{r^2}\eta_\theta\zeta_\theta\frac{\partial T}{\partial\zeta}\right)+\frac{\partial}{\partial\eta}\left(J\frac{1}{r^2}\eta_\theta\eta_\theta\frac{\partial T}{\partial\eta}\right)\\
&+\frac{1}{\xi}\frac{\partial}{\partial\xi}\left(J\xi\xi_z\xi_z\frac{\partial T}{\partial\xi}\right)+\frac{\partial}{\partial\xi}\left(J\xi\xi_z\zeta_z\frac{\partial T}{\partial\zeta}\right)+\frac{\partial}{\partial\xi}\left(J\xi\xi_z\eta_z\frac{\partial T}{\partial\eta}\right)\\
&+\frac{1}{\xi}\frac{\partial}{\partial\zeta}\left(J\xi\zeta_z\xi_z\frac{\partial T}{\partial\xi}\right)+\frac{\partial}{\partial\zeta}\left(J\xi\zeta_z\zeta_z\frac{\partial T}{\partial\zeta}\right)+\frac{\partial}{\partial\zeta}\left(J\xi\zeta_z\eta_z\frac{\partial T}{\partial\eta}\right)\\
&+\frac{\partial}{\partial\eta}\left(J\eta_z\xi_z\frac{\partial T}{\partial\xi}\right)+\frac{\partial}{\partial\eta}\left(J\eta_z\zeta_z\frac{\partial T}{\partial\zeta}\right)+\frac{\partial}{\partial\eta}\left(J\eta_z\eta_z\frac{\partial T}{\partial\eta}\right)
\end{aligned}
\tag{9}.
$$

In this analysis, fractional step method is utilized to solve these governing equations. Adams-Bashforth method is adapted for time advancement. The Crank-Nicholson scheme is applied only the circumferential constituent of the viscous terms in the Navier-Stokes and the energy equations in order to ensure a larger stability margin.

3.3 Boundary conditions

3.3.1 Boundary condition of the velocity

To derive the boundary condition of the velocity on the free surface, the balance between the shearing stress and the surface tension must be considered.

The relation between the shearing stress and the surface tension is shown in Fig. 2.

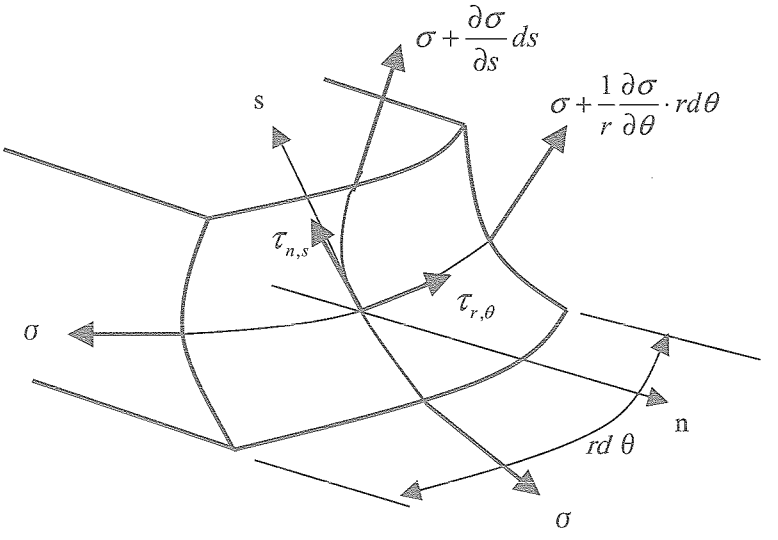

Figure 2: Stress balance between shearing stress and surface tension

From Fig. 2 the equations of the balance between the shearing stress and the surface tension are described as

$$\begin{cases} \tau_{n,s} \cdot rd\theta ds = \left\{ \left(\sigma + \dfrac{\partial \sigma}{\partial s} \cdot ds \right) - \sigma \right\} \cdot rd\theta \\ \tau_{r,\theta} \cdot rd\theta ds = \left\{ \left(\sigma + \dfrac{1}{r}\dfrac{\partial \sigma}{\partial \theta} \cdot rd\theta \right) - \sigma \right\} \cdot rds \end{cases} \tag{10}$$

Newton's law of viscosity is expressed as follows.

$$\begin{cases} \tau_{n,s} = \mu \left\{ \dfrac{\partial v_s}{\partial n} + \dfrac{\partial v_n}{\partial s} \right\} \\ \tau_{r,\theta} = \mu \left\{ \dfrac{1}{r}\dfrac{\partial v_r}{\partial \theta} + r\dfrac{\partial}{\partial r}\left(\dfrac{v_\theta}{r} \right) \right\} \end{cases} \tag{11}$$

From Eqs. (10) and (11), equation (12) is derived.

$$\begin{cases} \mu\left\{\dfrac{\partial v_s}{\partial n}+\dfrac{\partial v_n}{\partial s}\right\}=\dfrac{\partial \sigma}{\partial s} \\ \mu\left\{\dfrac{1}{r}\dfrac{\partial v_r}{\partial \theta}+r\dfrac{\partial}{\partial r}\left(\dfrac{v_\theta}{r}\right)\right\}=\dfrac{1}{r}\dfrac{\partial \sigma}{\partial \theta} \end{cases} \tag{12}$$

If the velocity on the free surface in the normal direction is assumed to be zero, equation (12) can be shown as follows.

$$\begin{cases} \mu\dfrac{\partial v_s}{\partial n}=\dfrac{\partial \sigma}{\partial s} \\ \mu\left\{\dfrac{1}{r}\dfrac{\partial v_r}{\partial \theta}+r\dfrac{\partial}{\partial r}\left(\dfrac{v_\theta}{r}\right)\right\}=\dfrac{1}{r}\dfrac{\partial \sigma}{\partial \theta} \end{cases} \tag{13}$$

Equation (11) can be non-dimensionalized as following equations.

$$\begin{cases} \dfrac{\partial v_s}{\partial n}=-\dfrac{\partial \sigma}{\partial s} \\ \dfrac{1}{r}\dfrac{\partial v_r}{\partial \theta}+r\dfrac{\partial}{\partial r}\left(\dfrac{v_\theta}{r}\right)=-\dfrac{1}{r}\dfrac{\partial \sigma}{\partial \theta} \end{cases} \tag{14}$$

In the equation of the relation between normal and tangential directions, the tangential velocity v_s is divided into radius and axial directions (See Fig. 3).

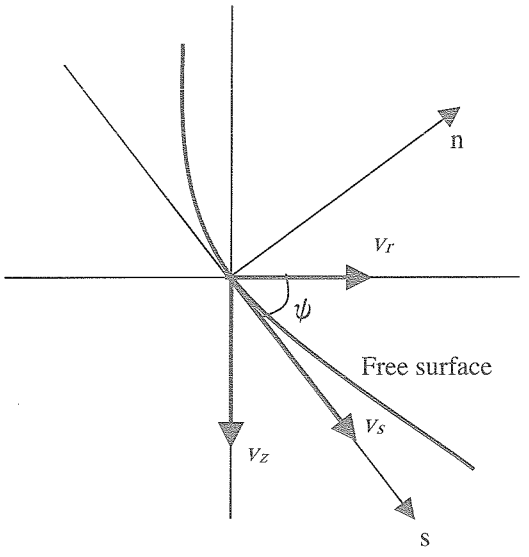

$$\begin{cases} v_r = v_s cos\varphi \\ v_z = v_s sin\varphi \end{cases} \tag{15}$$

$$\Leftrightarrow \begin{cases} v_s = \dfrac{v_r}{cos\varphi} \\ v_s = \dfrac{v_z}{sin\varphi} \end{cases} \tag{16}$$

$$\Leftrightarrow \begin{cases} \dfrac{\partial v_s}{\partial n}=\dfrac{\partial}{\partial n}\left(\dfrac{v_r}{cos\varphi}\right) \\ \dfrac{\partial v_s}{\partial n}=-\dfrac{\partial}{\partial n}\left(\dfrac{v_z}{sin\varphi}\right) \end{cases} \tag{17}$$

$$\Leftrightarrow \begin{cases} \dfrac{\partial}{\partial n}\left(\dfrac{v_r}{cos\varphi}\right)=-\dfrac{\partial T}{\partial s} \\ \dfrac{\partial}{\partial n}\left(\dfrac{v_z}{sin\varphi}\right)=-\dfrac{\partial T}{\partial s} \end{cases} \tag{18}$$

Figure 3: Velocity on the free surface

Generally the following relations are derived in the normal and tangential di rections.

[Normal Derivatives]

$$\begin{cases} \dfrac{\partial \phi}{\partial n^{(\xi)}} = \dfrac{1}{J\sqrt{\alpha}}\left(\alpha\phi_{\xi} - \beta\phi_{\eta}\right) \\ \dfrac{\partial \phi}{\partial n^{(\eta)}} = \dfrac{1}{J\sqrt{\gamma}}\left(-\beta\phi_{\xi} + \gamma\phi_{\eta}\right) \end{cases} \tag{19}$$

[Tangential Derivatives]

$$\begin{cases} \dfrac{\partial \phi}{\partial s^{(\xi)}} = \dfrac{1}{\sqrt{\alpha}}\phi_{\eta} \\ \dfrac{\partial \phi}{\partial s^{(\eta)}} = \dfrac{1}{\sqrt{\gamma}}\phi_{\xi} \end{cases} \tag{20}$$

where, $\alpha = r_{\eta}^2 + z_{\eta}^2, \quad \beta = r_{\xi}r_{\eta} + z_{\xi}z_{\eta}, \quad \gamma = r_{\xi}^2 + z_{\xi}^2$.

Using eq. (19), the equation of the stress balance in normal and tangential directions is obtained.

$$\frac{1}{J\sqrt{\alpha}}\left(\alpha\frac{\partial v_z}{\partial \xi} - \beta\frac{\partial v_z}{\partial \eta}\right) = -sin\varphi\frac{1}{\sqrt{\alpha}}\frac{\partial T}{\partial \eta} \tag{21}.$$

The axial velocity is derived from eq. (21). The radius velocity is derived from the relation of following equation.

$$v_r = \frac{cos\varphi}{sin\varphi}v_z \tag{22}.$$

On the other hand, the boundary condition of the circumferential velocity is defined by

$$\frac{1}{r}\frac{\partial v_r}{\partial \theta} + r\frac{\partial}{\partial r}\left(\frac{v_\theta}{r}\right) = -\frac{1}{r}\frac{\partial T}{\partial \theta} \tag{23}.$$

Equation (23) is transformed to the one in the computational domain by the Jacobian matrix as

$$\begin{aligned} &\frac{1}{r}\left(\xi_\theta\frac{\partial v_r}{\partial \xi} + \zeta_\theta\frac{\partial v_r}{\partial \zeta} + \eta_\theta\frac{\partial v_r}{\partial \eta}\right) + r\left(\xi_r\frac{\partial}{\partial \xi}\left(\frac{v_\theta}{r}\right) + \zeta_r\frac{\partial}{\partial \zeta}\left(\frac{v_\theta}{r}\right) + \eta_r\frac{\partial}{\partial \eta}\left(\frac{v_\theta}{r}\right)\right) \\ &\quad = -\frac{1}{r}\left(\xi_\theta\frac{\partial T}{\partial \xi} + \zeta_\theta\frac{\partial T}{\partial \zeta} + \eta_\theta\frac{\partial T}{\partial \eta}\right) \end{aligned} \tag{24}.$$

3.3.2 Boundary condition of the temperature

The condition of the heat transfer over the free surface is assumed to be adiabatic. Therefore the equation of the boundary condition of the temperature is

$$\frac{\partial T}{\partial n} = 0 \tag{25}.$$

Equation (25) is transformed by the Jacobian matrix as

$$\frac{\partial T}{\partial \xi}\frac{\partial \xi}{\partial n}+\frac{\partial T}{\partial \zeta}\frac{\partial \zeta}{\partial n}+\frac{\partial T}{\partial \eta}\frac{\partial \eta}{\partial n}=0. \tag{26}$$

To transform into the computational domain, equation (19) is utilized.

$$\frac{\partial T}{\partial n}=\frac{1}{J\sqrt{\alpha}}\left(\alpha\frac{\partial T}{\partial \xi}-\beta\frac{\partial T}{\partial \eta}\right) \tag{27}$$

3.3.3 Treatment of the liquid center axis

In this analysis the governing equations are described in the cylindrical coordinate. Therefore the center of the cylinder (r = 0) can not be solved directly by the present equation. This problem is solved by a method described below. The computational grid is fixed at the center.

The Navier-Stokes equation in the axial direction and the energy equation at the center are derived by azimuthal integration.

[Navier-Stokes equation of the liquid center]

$$\begin{aligned}
&r\frac{\partial v_z}{\partial t}+\frac{\partial}{\partial r}\left(rv_rv_z\right)+\frac{\partial}{\partial \theta}\left(v_\theta v_z\right)+\frac{\partial}{\partial z}\left(rv_zv_z\right)\\
&=-r\frac{\partial P}{\partial z}+\frac{Pr}{Ma}\left[\frac{\partial}{\partial r}\left(r\frac{\partial v_z}{\partial r}\right)+\frac{\partial}{\partial \theta}\left(\frac{1}{r}\frac{\partial v_z}{\partial \theta}\right)+\frac{\partial}{\partial z}\left(r\frac{\partial v_z}{\partial z}\right)\right]\\
\Rightarrow\ &\frac{\partial v_z}{\partial t}+\frac{\Delta\theta}{\pi\Delta r}\sum_{\theta=0}^{2\pi}\left(v_rv_z\right)+\frac{1}{\Delta z}\left[v_z^2\right]_0^{\Delta z}\\
&=-\frac{\partial P}{\partial z}+\frac{Pr}{Ma}\left[\frac{\Delta\theta}{\pi\Delta r}\sum_{\theta=0}^{2\pi}\frac{\partial v_z}{\partial r}\bigg|_{\Delta r}+\frac{1}{\Delta z}\left[\frac{\partial v_z}{\partial z}\right]_0^{\Delta z}\right]
\end{aligned} \tag{28}$$

[Energy equation]

$$\begin{aligned}
&r\frac{\partial T}{\partial t}+\frac{\partial}{\partial r}\left(rv_rT\right)+\frac{\partial}{\partial \theta}\left(v_\theta T\right)+\frac{\partial}{\partial z}\left(rv_zT\right)\\
&=\frac{1}{Ma}\left[\frac{\partial}{\partial r}\left(r\frac{\partial T}{\partial r}\right)+\frac{\partial}{\partial \theta}\left(\frac{1}{r}\frac{\partial T}{\partial \theta}\right)+\frac{\partial}{\partial z}\left(r\frac{\partial T}{\partial z}\right)\right]\\
\Rightarrow\ &r\frac{\partial T}{\partial t}+\frac{\Delta\theta}{\pi\Delta r}\sum_{\theta=0}^{2\pi}\left(v_rT\right)+\frac{1}{\Delta z}\left[v_zT\right]_0^{\Delta z}\\
&=\frac{1}{Ma}\left\{\frac{\Delta\theta}{\pi\Delta r}\sum_{\theta=0}^{2\pi}\frac{\partial T}{\partial r}\bigg|_{\Delta r}+\frac{1}{\Delta z}\left[\frac{\partial T}{\partial z}\right]_0^{\Delta z}\right\}
\end{aligned} \tag{29}$$

As for the radius and circumference velocity at the center, the velocity is evaluated by summed value over the surrounding mesh points (See Fig.4).

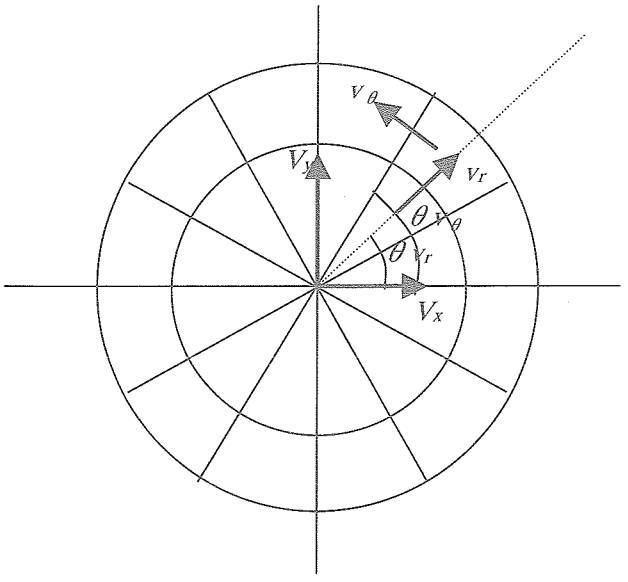

$$V_x = \sum_{\theta=0}^{2\pi} \left\{ v_r cos\theta_{v_r} + v_\theta cos\left(\theta_{v_\theta} + \frac{\pi}{2} \right) \right\}$$

$$V_y = \sum_{\theta=0}^{2\pi} \left\{ v_r sin\theta_{v_r} + v_\theta sin\left(\theta_{v_\theta} + \frac{\pi}{2} \right) \right\}$$

Figure 4: The velocity at the center axis

After the summation, the velocities V_x, V_y are divided into the radius and circumference components (v_r, v_θ) as follows;

$$v_r = \left[V_x cos\theta_{v_r} + V_y cos\left(\frac{\pi}{2} - \theta_{v_r} \right) \right] \frac{1}{nj}$$

$$v_\theta = \left[V_x \left(-sin\theta_{v_\theta} \right) cos + V_y sin\left(\frac{\pi}{2} - \theta_{v_\theta} \right) \right] \frac{1}{nj} \qquad (31).$$

Here, *nj* shows the division number of the circumference direction. This treatment at the center axis is also applied to the energy equation.

3.4 Free surface deformation

The stress balance over the free surface must be considered to compute the free surface shape. Along the interface between two immiscible fluids (1) and (2), the forces over the surface must be balanced. If the surface is plane and the surface tension is constant, the stress balance over the surface leads

$$\mathbb{S}^{(1)} \cdot \mathbf{n} = \mathbb{S}^{(2)} \cdot \mathbf{n} \qquad (32)$$

where S is the stress tensor and n is the unit normal vector directed out of liquid (1) into the ambient fluid (2). The each component in the stress tensor is described as

$$S_{i,j} = -P\delta_{i,j} + \mu e_{i,j} \qquad (33),$$

where $e_{i,j}$ can be expressed in the cylindrical coordinate as

$$e_{rr}=\frac{\partial v_r}{\partial r},\quad e_{\theta\theta}=\frac{1}{r}\frac{\partial v_\theta}{\partial \theta}+\frac{v_r}{r},\quad e_{zz}=\frac{\partial v_z}{\partial z},$$
$$e_{r\theta}=\frac{1}{2}\left\{r\frac{\partial}{\partial r}\left(\frac{v_\theta}{r}\right)+\frac{1}{r}\frac{\partial v_r}{\partial \theta}\right\},\quad e_{\theta z}=\frac{1}{2}\left\{\frac{1}{r}\frac{\partial v_z}{\partial \theta}+\frac{\partial v_\theta}{\partial z}\right\},\quad e_{r\theta}=\frac{1}{2}\left\{\frac{\partial v_r}{\partial z}+\frac{\partial v_z}{\partial r}\right\} \tag{34}$$

On the other hand, if the free surface has curvature and the surface tension varies along the interface, the equation of the stress balance becomes [8]

$$\mathbb{S}^{(1)}\cdot\mathbf{n}+\sigma(\nabla\cdot\mathbf{n})\mathbf{n}-(\mathbf{I}-\mathbf{nn})\cdot\nabla\sigma=\mathbb{S}^{(2)}\cdot\mathbf{n} \tag{35}$$

where, I is the identity matrix. The element σ (∇ · n) in the second term is so-called Laplace pressure. The mean curvatures of the interface,

$$\nabla\cdot\mathbf{n}=\frac{1}{R_1}+\frac{1}{R_2} \tag{36}$$

can be expressed as the sum of the inverse principle radii of curvatures R_1 and R_2. The mean curvatures of the interface can be described with Cartesian coordinate system as follows;

$$\begin{aligned}\nabla\cdot\mathbf{n}=\frac{-1}{R^3N^3}\Bigg[\quad & R\frac{\partial^2R}{\partial z^2}\left\{R^2+\left(\frac{\partial R}{\partial\theta}\right)^2\right\}\\ & +2\frac{\partial R}{\partial z}\frac{\partial R}{\partial\theta}\left(\frac{\partial R}{\partial z}\frac{\partial R}{\partial\theta}-R\frac{\partial^2R}{\partial z\partial\theta}\right)\\ & -\left\{1+\left(\frac{\partial R}{\partial z}\right)^2\right\}\left\{R^2+2\left(\frac{\partial R}{\partial\theta}\right)^2-R\frac{\partial^2R}{\partial\theta^2}\right\}\Bigg]\end{aligned} \tag{37}$$

where, $N=\left[1+\left(\frac{\partial R}{\partial z}\right)^2+\frac{1}{R^2}\left(\frac{\partial R}{\partial\theta}\right)^2\right]^{\frac{1}{2}}$

The second term in the left hand side of equation (35) indicates the surface force acting tangentially originated from the surface tension σ. The operator I-nn represents the orthogonal projection of a vector onto the tangent plane defined by n.

Equation (35) can be non-dimensionalized using the scale as Table 1.

$$\mathbb{S}^{(1)}\cdot\mathbf{n}+\left(\frac{1}{Ca}-T\right)(\nabla\cdot\mathbf{n})\mathbf{n}-(\mathbf{I}-\mathbf{nn})\cdot\nabla T=\mathbb{S}^{(2)}\cdot\mathbf{n} \tag{38}$$

Here, the dimensionless parameter is called the Capillary number, defined as

$$Ca=\frac{\sigma_T\Delta T}{\sigma_0} \tag{39}$$

From these equations, the equation of the stress balance is led in the three directions. Since the two directions of the curvature exist in the three dimension, the two tri-diagonal matrices must be considered for axial and circumferential directions. The tri-diagonal equations are indicated below.

[Radius direction]

$$\frac{\partial^2 R}{\partial z^2} = \frac{-R^3 N^3}{R\left\{R^2 + \left(\partial R/\partial\theta\right)^2\right\}\left(1/Ca - T\right)}\Bigg[\quad Re\left(P^{(1)} - P^{(2)}\right) - \frac{Bo}{Ca}\left(H - z\right) - \frac{\partial v_r}{\partial r}$$
$$- \frac{1}{2}\left\{r\frac{\partial}{\partial r}\left(\frac{v_\theta}{r}\right) + \frac{1}{r}\frac{\partial v_r}{\partial\theta}\right\}\frac{n_\theta}{n_r} - \frac{1}{2}\left(\frac{\partial v_r}{\partial z} + \frac{\partial v_z}{\partial r}\right)\frac{n_z}{n_r}$$
$$- \frac{1 - n_r^2}{n_r}\frac{\partial T}{\partial r} + n_\theta\frac{1}{r}\frac{\partial T}{\partial\theta} + n_z\frac{\partial T}{\partial z}\Bigg]$$
$$+ \frac{1}{R\left\{R^2 + \left(\partial R/\partial\theta\right)^2\right\}}\Bigg[-2\frac{\partial R}{\partial z}\frac{\partial R}{\partial\theta}\left(\frac{\partial R}{\partial z}\frac{\partial R}{\partial\theta} - R\frac{\partial^2 R}{\partial z\partial\theta}\right)$$
$$+ \left\{1 + \left(\frac{\partial R}{\partial z}\right)^2\right\}\left\{R^2 + 2\left(\frac{\partial R}{\partial\theta}\right)^2 - R\frac{\partial^2 R}{\partial\theta^2}\right\}\Bigg] \tag{40}$$

[Circumferential direction]

$$\frac{\partial^2 R}{\partial\theta^2} = \frac{-R^3 N^3}{R\left\{R^2 + \left(\partial R/\partial z\right)^2\right\}\left(1/Ca - T\right)}\Bigg[\quad Re\left(P^{(1)} - P^{(2)}\right) - \frac{Bo}{Ca}\left(H - z\right) - \frac{\partial v_r}{\partial r}$$
$$- \frac{1}{2}\left\{r\frac{\partial}{\partial r}\left(\frac{v_\theta}{r}\right) + \frac{1}{r}\frac{\partial v_r}{\partial\theta}\right\}\frac{n_\theta}{n_r} - \frac{1}{2}\left(\frac{\partial v_r}{\partial z} + \frac{\partial v_z}{\partial r}\right)\frac{n_z}{n_r}$$
$$- \frac{1 - n_r^2}{n_r}\frac{\partial T}{\partial r} + n_\theta\frac{1}{r}\frac{\partial T}{\partial\theta} + n_z\frac{\partial T}{\partial z}\Bigg]$$
$$+ \frac{1}{R\left\{R^2 + \left(\partial R/\partial z\right)^2\right\}}\Bigg[-R\frac{\partial^2 R}{\partial z^2}\left\{R^2 + \left(\frac{\partial R}{\partial\theta}\right)^2\right\}$$
$$- 2\frac{\partial R}{\partial z}\frac{\partial R}{\partial\theta}\left(\frac{\partial R}{\partial z}\frac{\partial R}{\partial\theta} - R\frac{\partial^2 R}{\partial z\partial\theta}\right)\Bigg]$$
$$+ \frac{2}{R}\left(\frac{\partial R}{\partial\theta}\right)^2 + R \tag{41}$$

In addition to these tri-diagonal equations, the constant volume equation is solved to maintain the volume of the liquid bridge.

$$\int_0^H\int_0^{2\pi}\frac{1}{2}R^2 d\theta dz = V \tag{42}$$

The position of the free surface R can be obtained by using Tri-Diagonal Matrix Algorithm (TDMA) in the axial and circumferential directions. [10]

4. RESULTS

Calculation of high Pr fluid needs fine grid in order to researches its quite thin thermal boundary layer. We perform the simulation with 2cSt silicone oil (Pr = 28.11), aspect ratio Γ= 1.0 and volume ratio = 1.0 under the zero gravity. The calculation gird points are increased up to (r·θ·z) = (56×32×70) with uniform size mesh. In the medium Pr case, we employed the grids in the last annual reports.

4.1 The effects of DSD on the flow field and the critical value

The steady flow states in the cases with and without the DSD are discussed. Temperature and velocity distributions in r-z plane, and those over the free surface are shown in fig.5 and fig.6, respectively. Those figure indicate the flow states at Ma = 20,000. No significant differences in those distributions can have seen in both cases. As for the case with DSD, the liquid bridge deformed statically from the straight cylinder as the initial shape. Statically deformed free surface and the pressure distribution over the free surface under the same conditions of figs.5 and 6 are shown in fig.7.

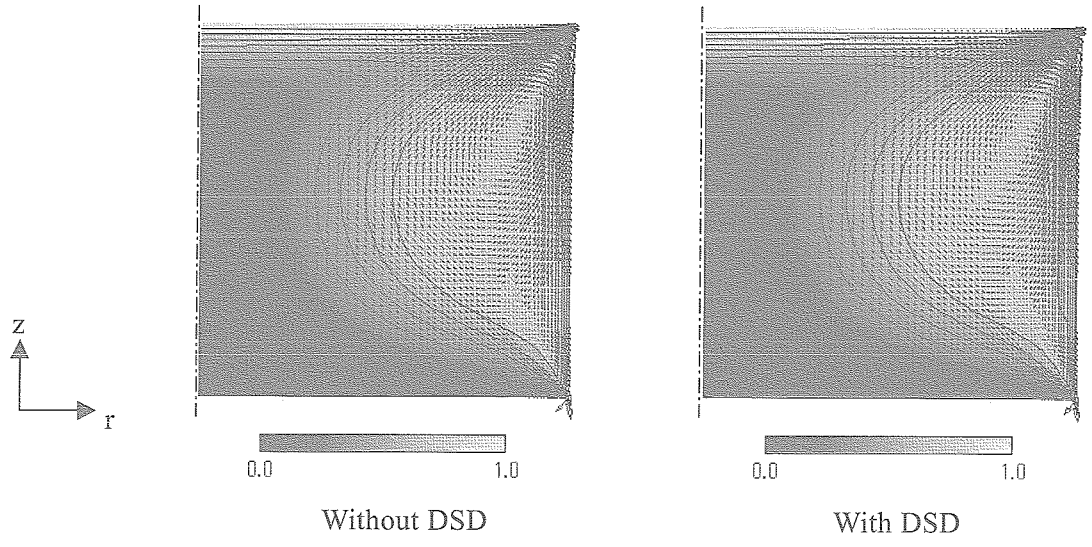

Figure 5: Temperature and velocity distribution for Ma = 30,000 with and without DSD.

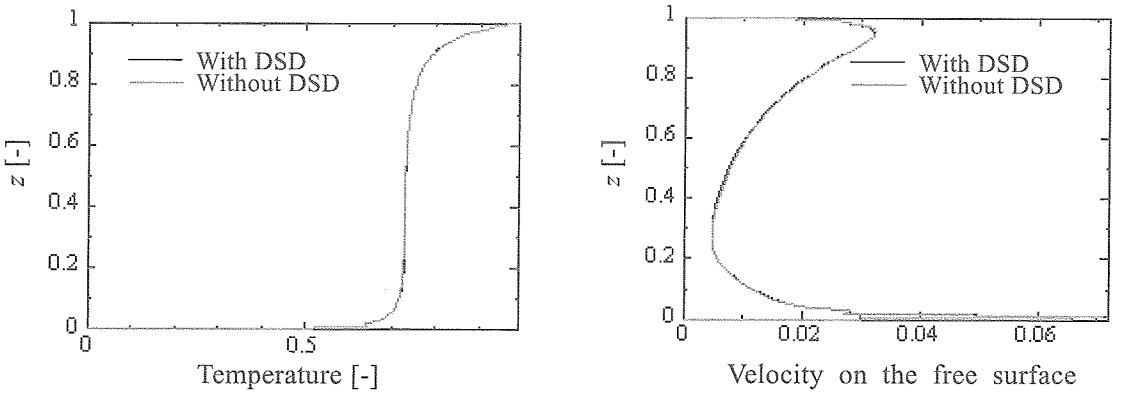

Figure 6: Free surface shape and pressure variation on the free surface for 2cSt silicone oil (Pr = 28.11), Ma= 30,000.

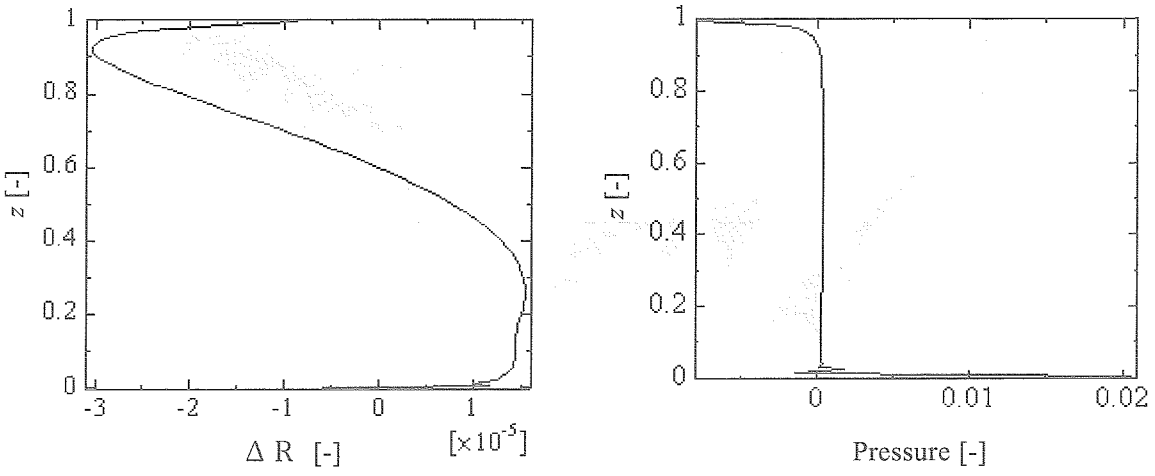

Figure 7: Free surface shape and pressure variation on the free surface for 2cSt silicone oil (Pr = 28.11), Ma = 30,000.

We evaluate the critical Marangoni numbers in the cases with and without DSD. Figure 8 shows the azimuthal velocity variation on the free surface at mid-height of the liquid bridge for both cases. Table 4 exhibits the evaluated value of Ma_c. In the case of high Pr fluid, the Ma_c with DSD shows a slightly lower value than the one without DSD. This tend is different from that in the case of medium Pr fluid as indicated in the last annual report; the Mac with DSD is almost equal to that without DSD.

At $Ma > Ma_c$, the flow exhibits a transition from the 2D steady to the 3D oscillatory flow in the both cases with and without DSD. It is noted that there exists a difference in the flow field after the transition; in the case without DSD, the flow changes into the standing-wave flow first, and then into the traveling-wave one soon. In the case with DSD, on the other hand, after exhibiting the standing-wave flow, that flow regime maintains for longer period. This can be indicated by monitoring. The azimuthal velocity and the temperature variations on the free surface at mid-height as shown in Fig.10. This figure shows the variations for Ma = 40,000. The black line indicates the value at $\theta = 1/4\pi$, which corresponds to the node point of the temperature and the anti-node point of the azimuthal velocity in the standing wave oscillation. On the other hand, the gray line indicates the value at $\theta = 0$, the anti-node point of the temperature and the node point of the azimuthal velocity. From this figure, the flow exhibits the standing wave flow at the early stage of the oscillation. The temperature and the azimuthal velocity of the node point are increasing. After all, the amplitudes of black and gray lines become equal, and the flow exhibit the traveling wave flow. With DSD, however, the temperature and the azimuthal velocity of the node point are not increasing but stable (Fig. 10(b)). With DSD, therefore, the flow field stays at standing wave flow for a long time.

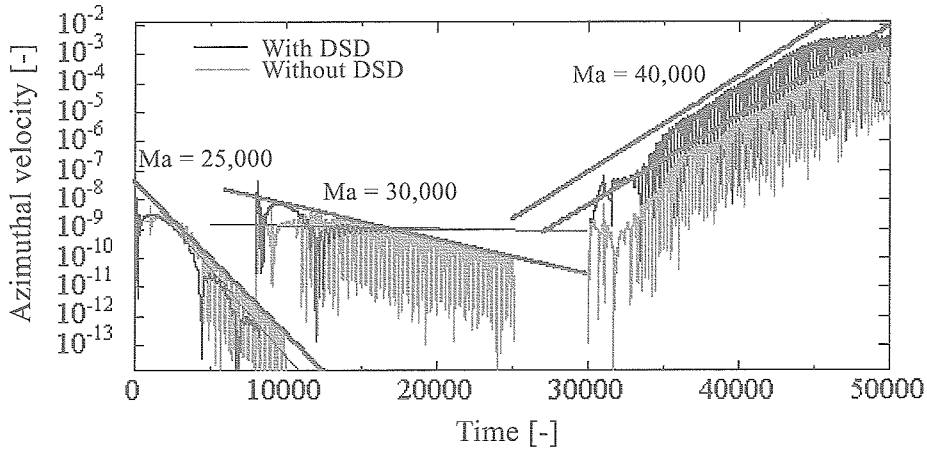

Figure 8: Azimuthal velocity variations for 2cSt silicone oil (Pr = 28.11), Ma = 25,000 ~ 40,000 with and without DSD

Table 4: Critical Marangoni number

2cSt silicone oil	Without DSD	With DSD
Ma_c	32,400	30,300

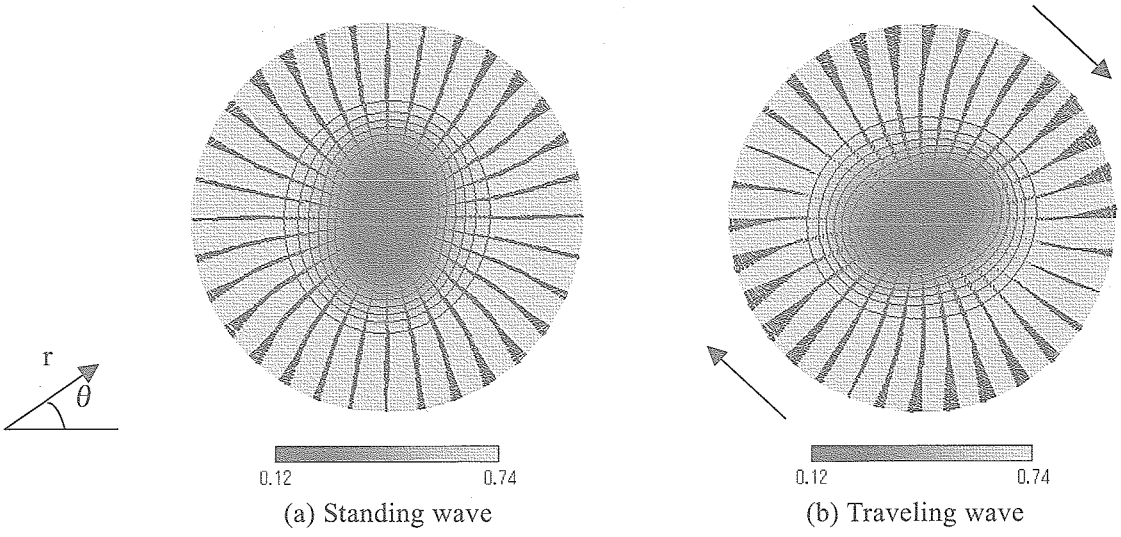

Figure 9: Temperature and velocity distributions in the standing wave (a) and traveling wave (b) oscillation, 2cSt silicone oil (Pr = 28.11), Ma = 40,000 without DSD in r - θ place at mid-height.

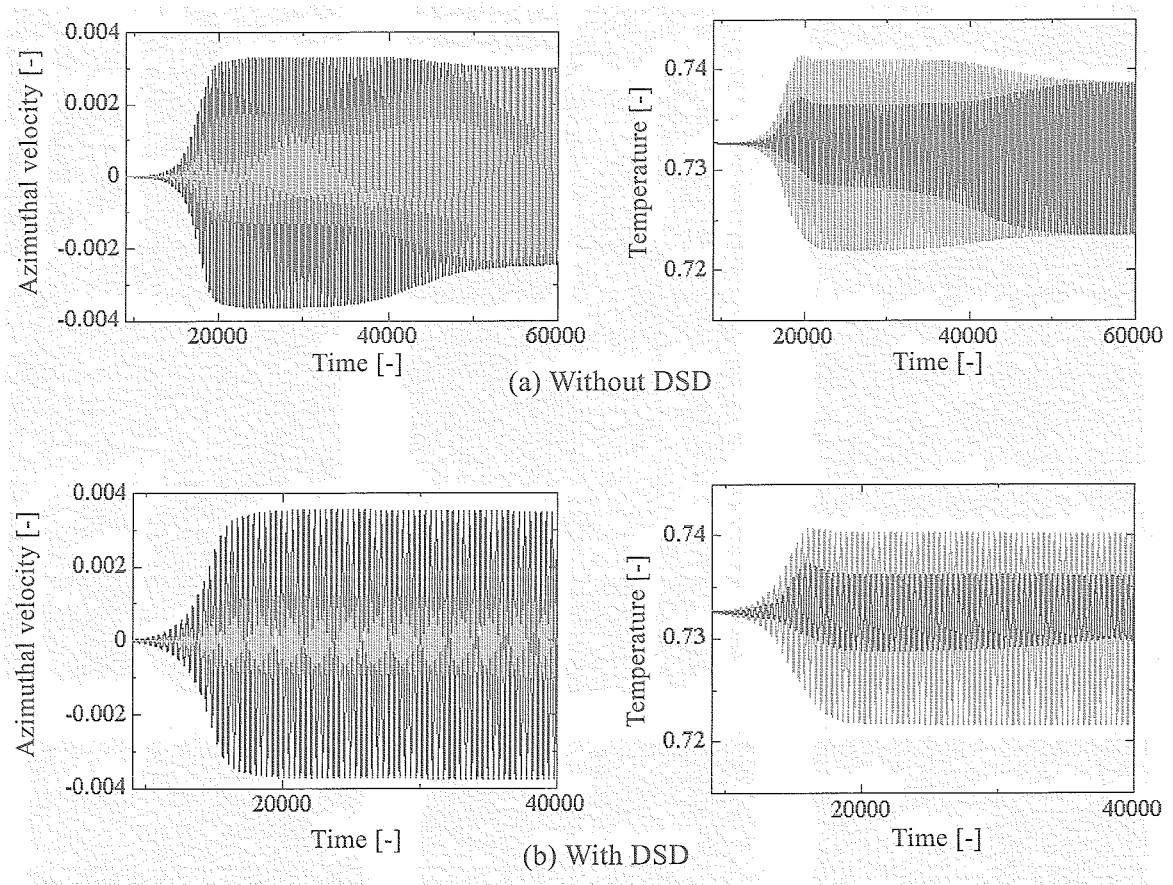

Figure 10: Azimuthal velocity and temperature variations at mid-height for 2cSt silicone oil (Pr = 28.11), Ma = 40,000. (a): without DSD, (b): with DSD. (black: $\theta = 1/4\pi$, gray: $\theta = 0$)

4.2 Spatiotemper al flow in the oscillatory state

Figure 11 shows the spatiotemporal correlati on among the free surface deformation, the temperature and the pressure variations for the traveling wave state. Fluctuation of the free surface displacement from the initial position is magnified in 10^3 times. The difference from medium Pr fluid appears in this figure; as the fluid at lower temp reaches the free surface, the pressure in the vicinity of the free surface rises, and the surface expands. On the other hand, as the fluid at higher temp reaches the free surface, the pressure in the vicinity of the free surface falls, and the surface become concaved. Figure 12 shows the mutual correlations among the dynamic free surface deformation, the temperature, and the absolute axial velocity in the traveling-wave state at the different height. These figures show one cycle of oscillation in the traveling wave state. A phase lag of about π exists between the temperature difference and the surface deformation at any heights. Nishino et al. exhibited this correlation through the experiment (Figure 13(a)). The present results show a good agreement with the experimental results as shown in Fig.13.

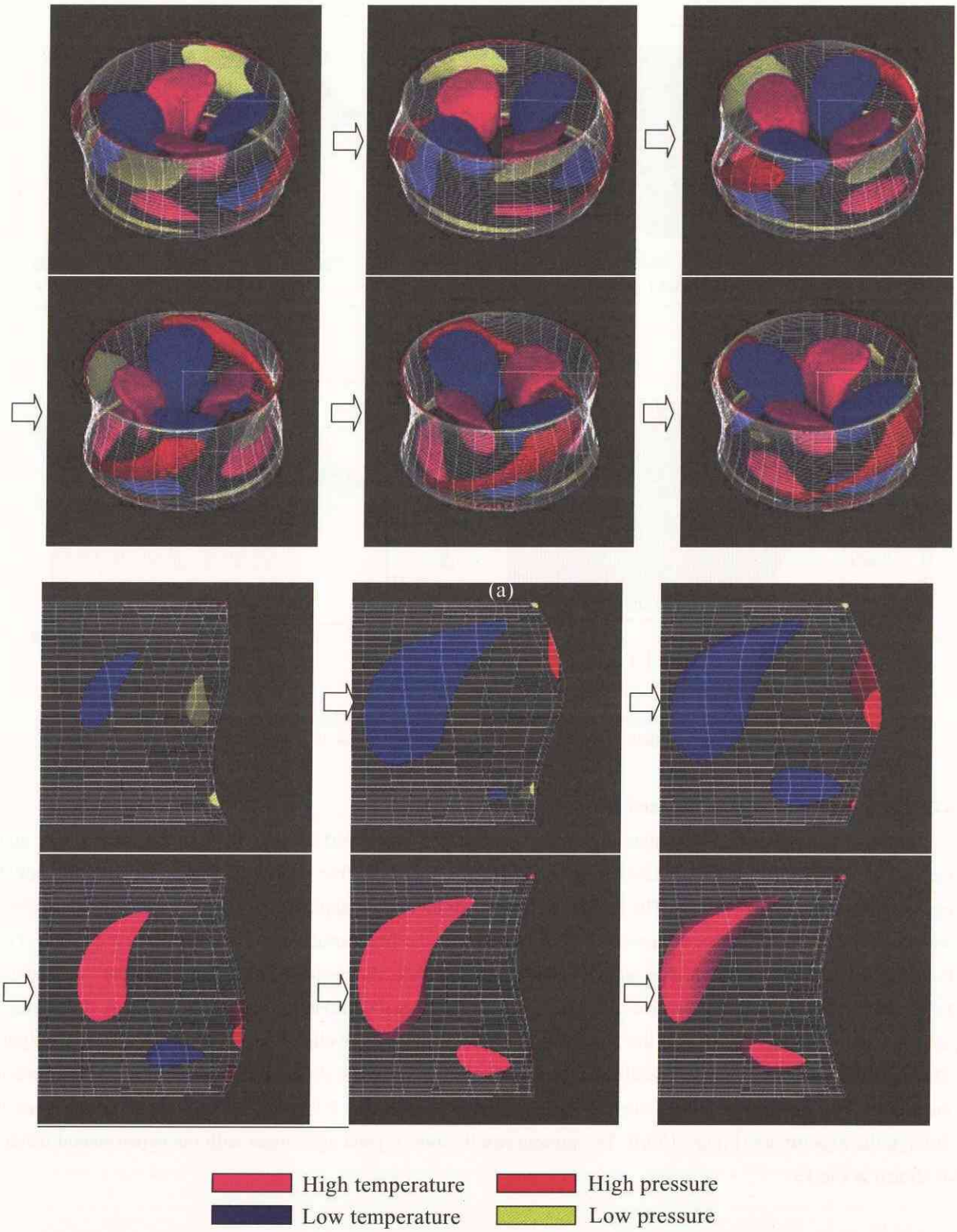

Figure 11: Bird's-eye view of traveling wave os cillation (a) and with fluctuations of temperature and pressure, in r – z place (b), 2cSt silicone oil (Pr = 28.11), Ma = 40,000. (DSD is magnified by a factor of 10^3)

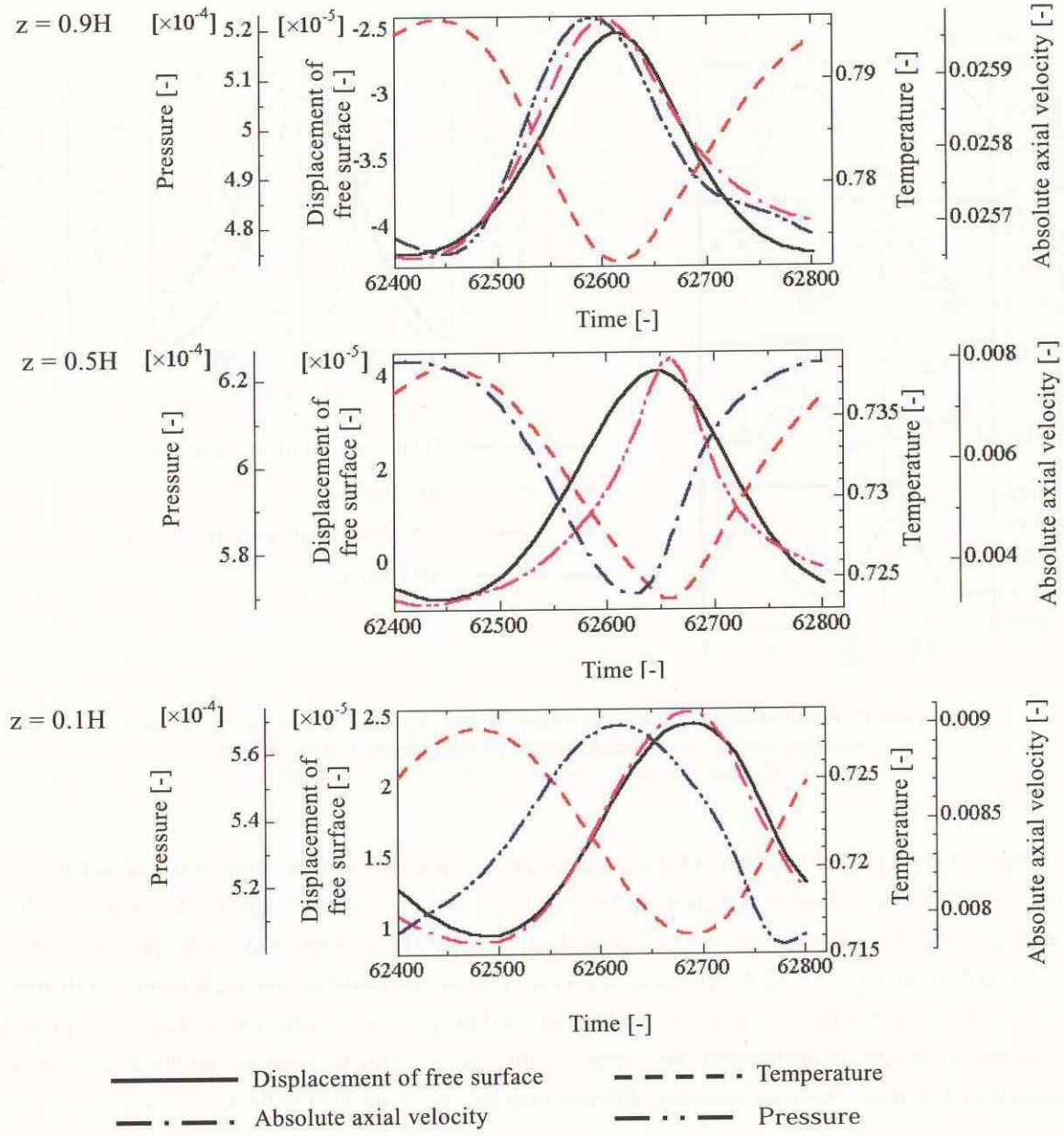

Figure 12: Relation between the surface deformat ion, pressure, temperature and absolute axial velocity near the both disks and at mid-height with DSD, 2cSt silicone oil, traveling wave oscillation, Ma = 40,000.

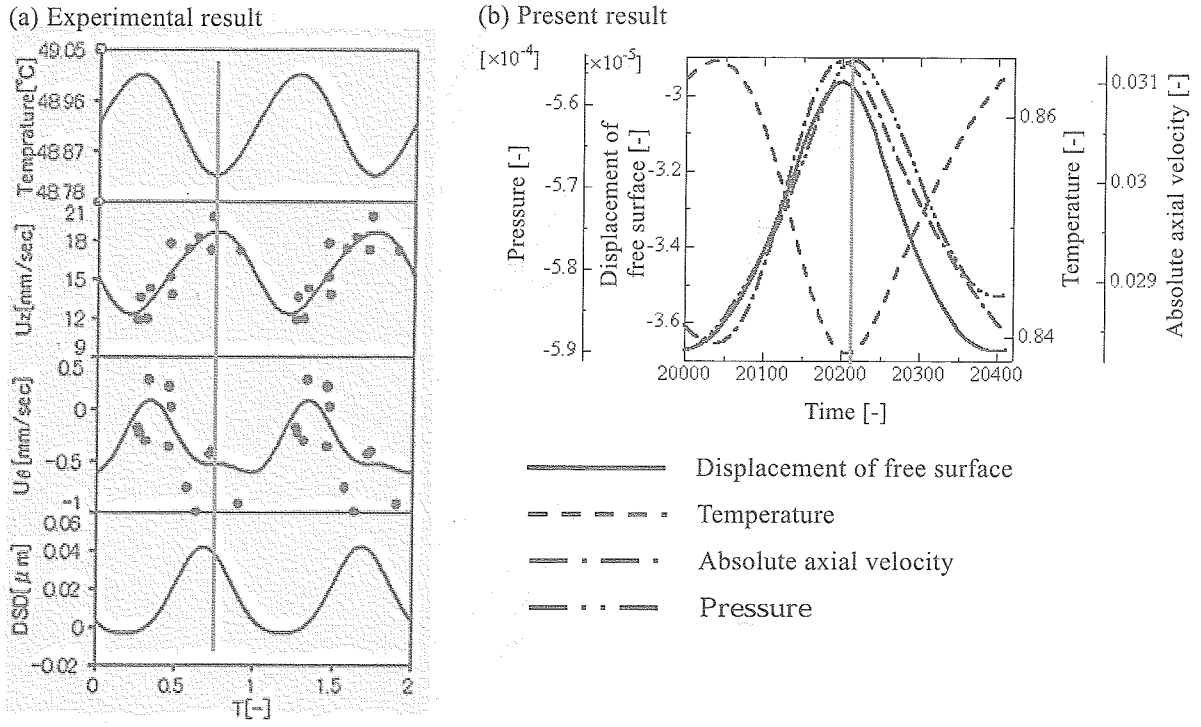

Figure 13: Relation between surface deformatio n, pressure, temperature and absolute axial velocity.z=0.96H, traveling wave oscillat ion, 2cSt silicone oil, Ma = 40,000.
(a): Experimental result (Nishino et al.), (b): Present result

Figure 14 shows the fluctuations of the temperat ure, the pressure and the azimuthal component of the velocity over the free surface in θ-z plane for the standing wave state. The azimuthal velocity vectors direct towards the coldest zone, as seen in the case of medium Pr fluid. The fluctuation of the temperature indicates meandering distribution at $z \sim 0.2\,H$. The fluctuation of the pressure also indicates the meandering distribution.

Figure 15 shows the fluctuations of the temperat ure and the pressure over the free surface in θ-z plane for the traveling wave state. In the traveling wave state, the fluctuations of the temperature and the pressure twist in the azimuthal directions. This phenomenon is different from the case of medium Pr fluid.

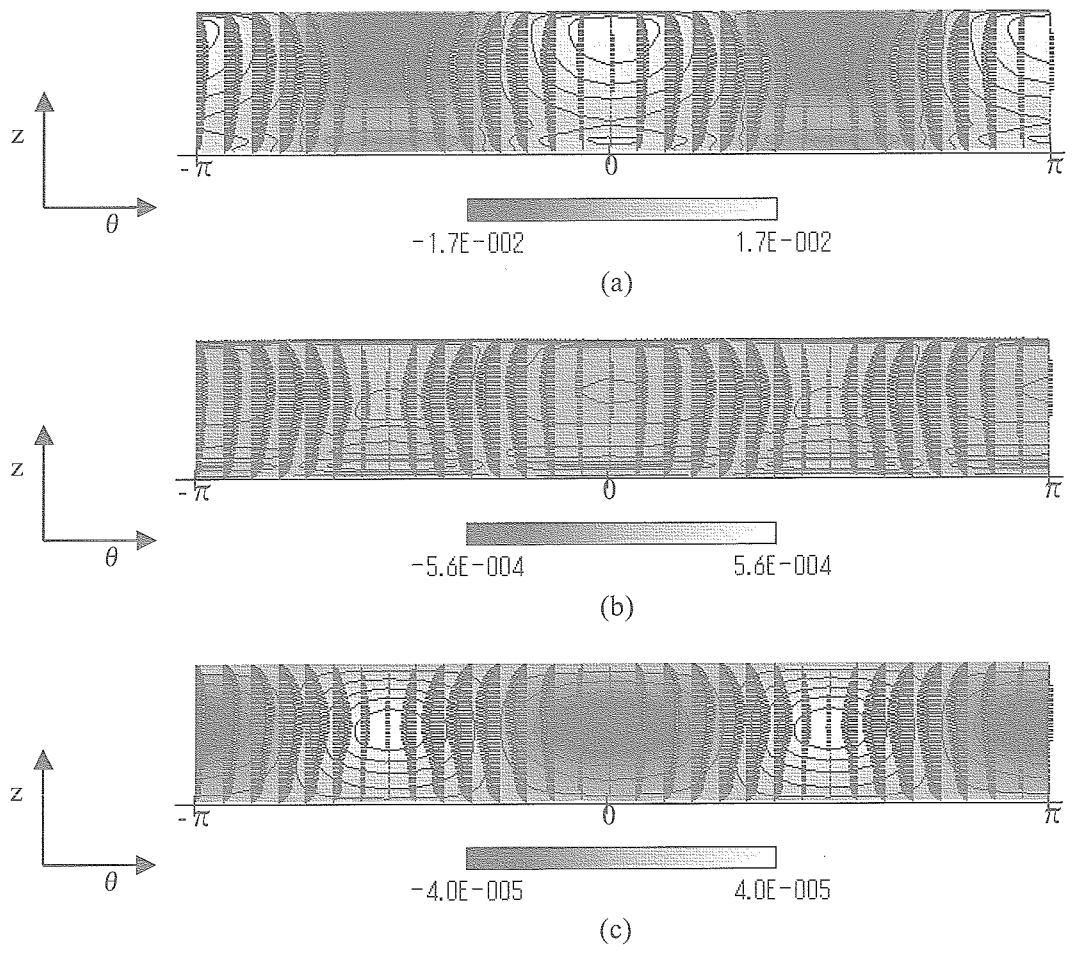

Figure 14: The fluctuations of the (a)temperature, (b)pressure, (c)surface deformation and the azimuthal velocity over the free surface with DSD in the standing wave in θ-z plane for Ma = 40,000, 2cSt silicone oil.

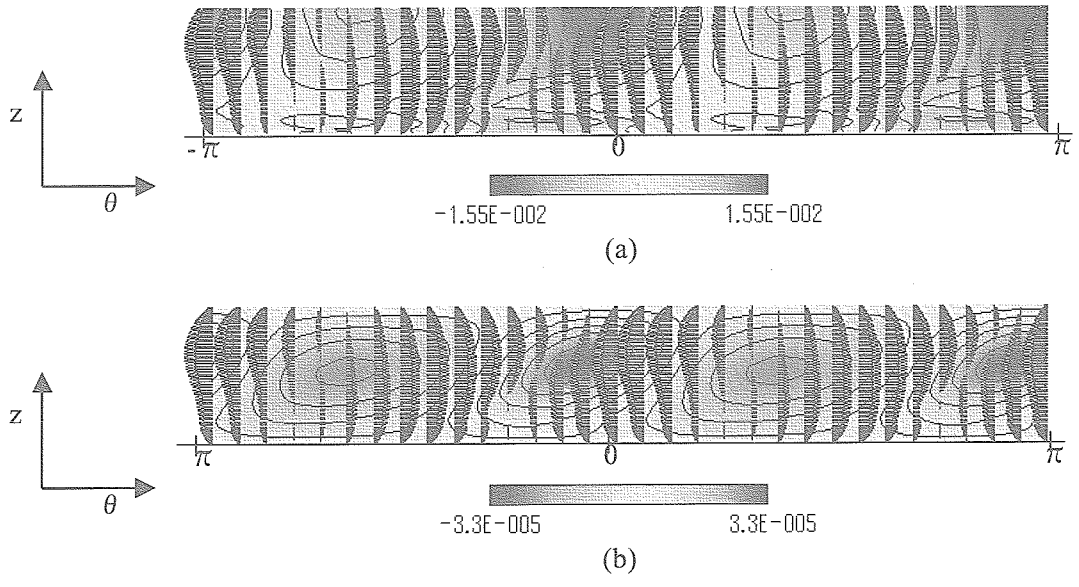

Figure 15: The fluctuations of the (a)temperature , (b)pressure and the azimuthal velocity over the free surface with DSD in the traveling wave in θ-z plane for Ma = 40,000, 2cSt silicone oil.

4.3 Comparison of the flow fields between the medium and high Pr fluid cases

In this section, the flow field of high Pr fluid is compared with that of low Pr fluid. Figure 16 shows the static free surface deformations in the case of the 2D steady flow. The free surface near the hot disk is concaved by low pressure due to Marangoni convection, and the one near the cold disk is expanded by high pressure in both cases. In the case of silicone oil, however, the free surface near the upper disk is widely concaved. Compared with the result of acetone the velocity near the upper disk is larger because of the steeper temperature gradient. The fluid vortex shifts up and the return-flow are strong.

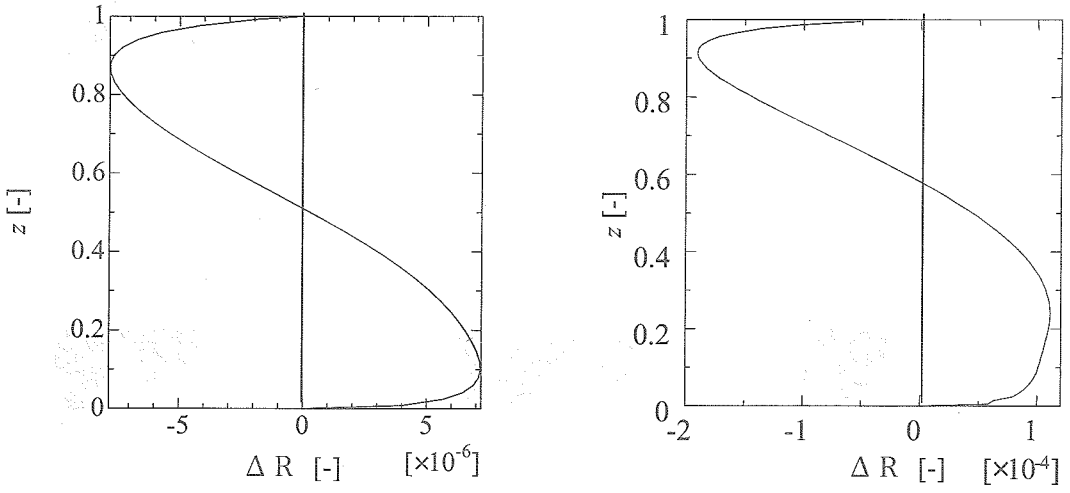

Figure 16: Free surface shape variations on the free surface (a): Acetone, Re = 900. (b): 2cSt silicone oil, Re = 890.

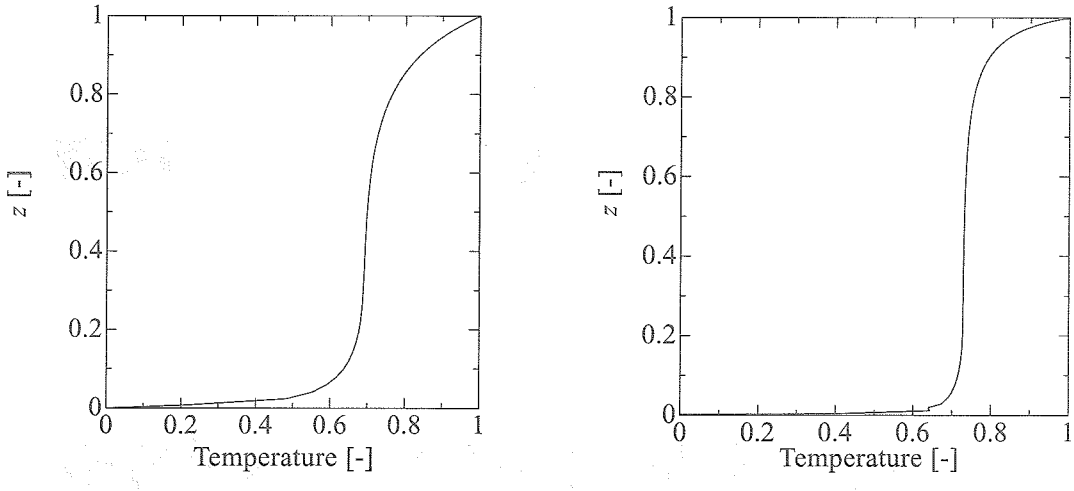

Figure 17: Temperature variations on the free surface (a): Acetone, Re = 900. (b): 2cSt silicone oil, Re = 890.

Figures 18 and 19 show the mutual correlations among the free surface deformation, the temperature and the pressure variations for the traveling wave state in the cases of 2cSt silicone oil and acetone, respectively. In both figure of medium and high Pr fluid, a phase lag exists between the temperature difference and the surface deformation. In case of high Pr fluid, this lag is about π. On the other hand, in case of medium Pr fluid, this lag is about $\pi/2$. It is conceived that the difference of a phase lag relates to height of the return-flow reaching. Figure 20

shows temperature and velocity distributions near the hot corner, in the r – z plane. Figure 21 shows fluctuations of the temperature and the velocity over the free surface in θ - z plane in a range of π/2 in θ. In the case of medium Pr fluid, low temperature field reaches widely to the free surface near upper disk. In the case of high Pr fluid, on the other hand, reaching range is narrow. Figure 21 shows that low temperature range is narrow near the upper disk. In medium Pr fluid, a phase relationship of high Pr fluid near the upper disk appears at little far from the upper disk.

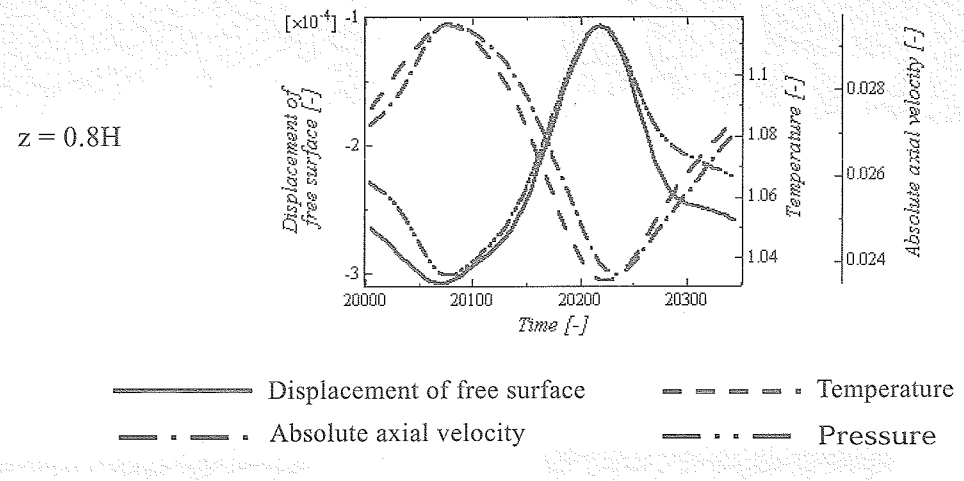

Figure 18: Relation between the surface deformation, pressure, temperature and absolute axial velocity near the both disks and at mid-height with DSD, 2cSt silicone oil, traveling wave oscillation, Ma = 40,000.

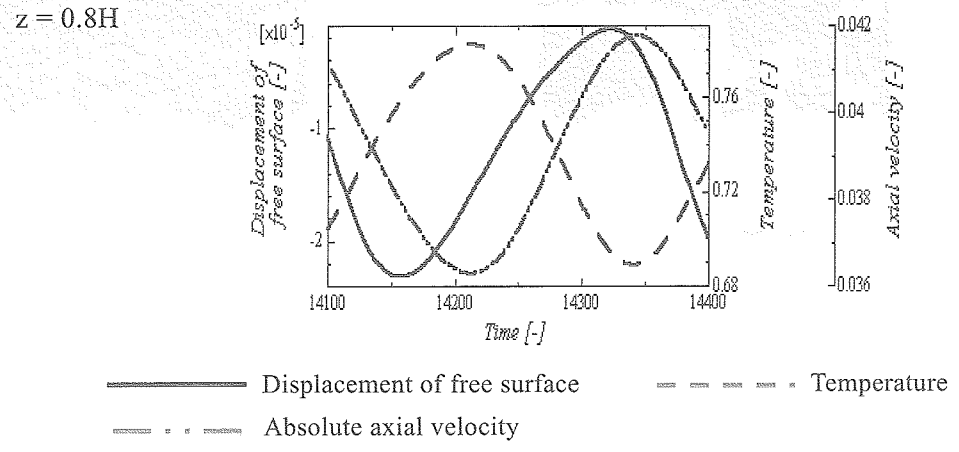

Figure 19: Relation between the surface deformation, temperature and absolute axial velocity at z = 0.8H with DSD, acetone, traveling wave oscillation, Re = 1,300.

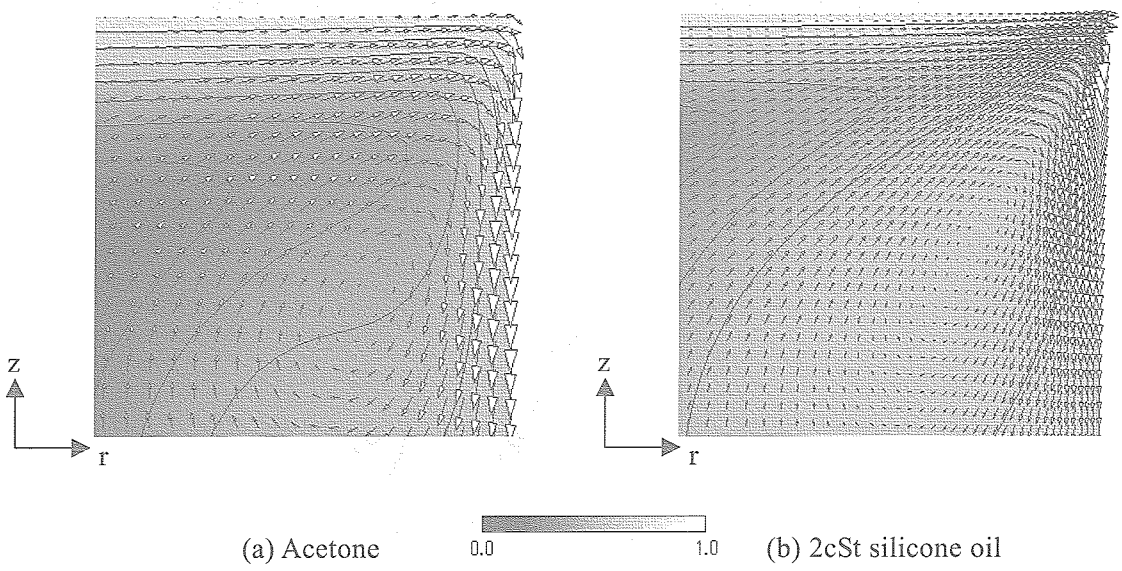

Figure 20: Temperature and velocity distributions near the hot corner, r – z plane.
(a): Acetone, Re = 1,300. (b): 2cSt silicone oil, Re = 1,440.

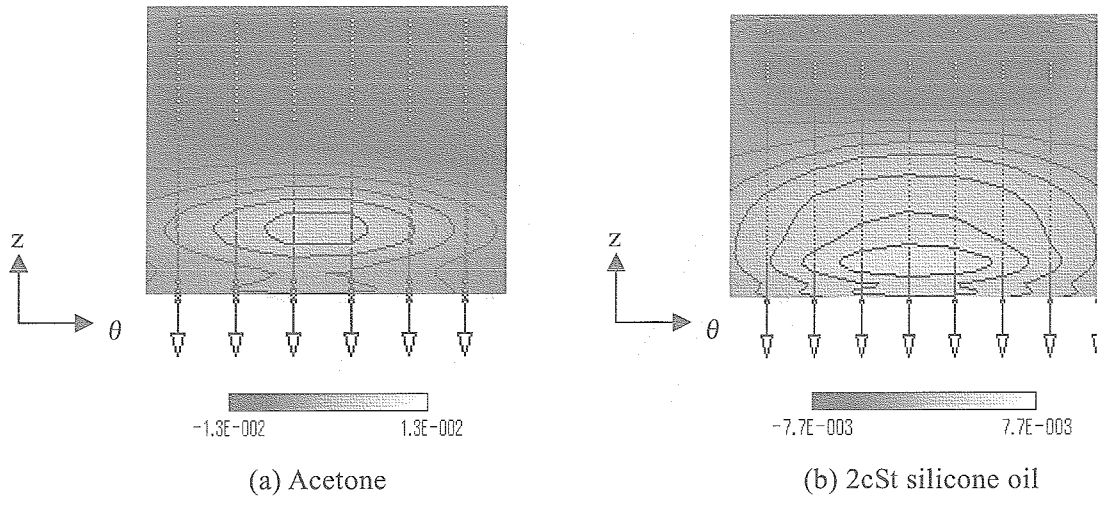

Figure 21: Fluctuations of the temperature and the velocity over the free surface in the standing wave oscillation in θ-z plane (π/2).
(a): Acetone, Re = 1,300. (b): 2cSt silicone oil, Re = 1,440.

5. CONCLUSIONS

(1) In the case of high Pr fluid, traveling flow with DSD using finer grids is obtained.

(2) The obtained critical Marangoni number in the case with DSD is smaller than the one without DSD.

(3) Mutual relation among DSD, temperature, pressure and axial velocity is obtained and is in good agreement with the experimental result near the hot corner (Nishino et al.).

(4) The differences of the oscillatory flow fields between the cases of acetone and of 2cSt silicone oil are indicated.